

# Fluorescence microscopy investigations of ligand propagation and accessibility under adherent cells

Jody L. Swift<sup>a)</sup>

Department of Chemistry, McGill University, 801 Sherbrooke Street West, Montréal, Québec H3A 2K6, Canada

Mikhail Sergeev

Department of Physics, McGill University, 3600 University Street, Montréal, Québec H3A 2T8, Canada

Paul W. Wiseman<sup>b)</sup>

Department of Chemistry and Physics, McGill University, 801 Sherbrooke Street West, Montréal, Québec H3A 2K6, Canada

(Received 25 September 2010; accepted 5 November 2010; published 14 December 2010)

Fluorescence microscopy methods including total internal reflection fluorescence and confocal laser scanning microscopy have played a major role in modern cell biology research by permitting imaging of fluorescently tagged macromolecules in living cells. These methods are often used to examine the initial events in signal transduction, which involve interactions occurring between membrane receptors and ligands such as antibodies and growth factors. Most quantitative biophysical applications using these fluorescence imaging methods, including ligand binding assays, are based on the assumption that the fluorophore label of interest has equal access to all areas of the membrane on the cell. Our findings suggest that there is limited accessibility of fluorophores ( $25 \pm 2\%$ ) under the basal membrane of adherent CHO-K1 cells expressing epidermal growth factor receptor plated on a bare glass in standard two-dimensional tissue cultures. The authors present a detailed study of the extent to which a small fluorescent dye molecule (Alexa 647) is able to propagate under the basal membrane of cells plated on a variety of biologically compatible substrates: fibronectin, bovine serum albumin, poly-*d*-lysine, collagen I, collagen IV, Geltrex™, and fibronectin such as binding polymer. For nonspecific dye propagation the best overall accessibility was achieved using a thin layer preparation of a commercially available basement membrane matrix, Geltrex™ ( $67 \pm 8\%$ ). Coupling of a specific high affinity ligand (epidermal growth factor) to the dye did result in a moderate increase in propagation for most substrates examined. Despite the overall increase in propagation for most substrates (60%–80%), large areas under the central regions of the adherent cells still remained inaccessible to the fluorescently labeled ligand. More importantly, the presence of the specific ligand did not result in consistent increase in ligand propagation. Taken together these results suggest that the reduced accessibility is not exclusively due to steric effects, and the chemistry of both the ligand and the substrate may be important when working under conditions of reduced dimensionality. © 2010 American Vacuum Society.

[DOI: 10.1116/1.3523470]

## I. INTRODUCTION

Technical advancements in the field of optical microscopy have had an enormous impact in cell and neural biology as well as live cell biophysics. It is now possible to visualize, with reasonably high resolution, dynamic processes occurring on the cell membrane, including but not limited to diffusion, ligand-receptor binding,<sup>1</sup> assembly and disassembly of cellular adhesions,<sup>2</sup> receptor clustering,<sup>3,4</sup> and receptor internalization.<sup>5</sup> Despite our fundamental knowledge of the basic components of cell membranes, the understanding of how these components dynamically participate in communication (cell to cell and cell to environment), signaling, and transport is still incomplete, but such mechanisms are of great interest for many disciplines.<sup>6</sup> Many of the microscopy

methods used to study cellular membrane dynamics, including confocal laser scanning microscopy (CLSM), spinning disk, and total internal reflection fluorescence (TIRF), are applied to two-dimensional (2D) tissue culture cell systems. In these cases samples are prepared on coated glass substrates, making the basal membrane (BM) the one that is often examined.<sup>7</sup> (We use the term basal membrane to indicate the membrane proximal to the glass interface, but it does not imply functional polarization of the cell as for epithelial cells.) For TIRF applications, the excitation laser light extends only to within  $\sim 100$  nm of the glass surface, and restricts interrogations almost exclusively to the basal membrane. Spatial fluorescence intensity fluctuation methods such as image correlation spectroscopy (ICS)<sup>3,8,9</sup> often require the examination of large flat, homogenous areas, making the basal membrane of adherent cells ideal for these techniques. Whether you are studying processes such as ligand-induced receptor clustering or simply labeling a component

<sup>a)</sup>Electronic mail: jody.swift@mail.mcgill.ca

<sup>b)</sup>Electronic mail: paul.wiseman@mcgill.ca

of the membrane, it is essential that all areas of the basal membrane are accessible to the ligand/label in order to study the system under equilibrium conditions with equal binding probabilities.

In our own basal membrane studies of epidermal growth factor receptor (EGFR) clustering in CHO-K1 cells, we observed that not all areas of cell are activated in a uniform manner. Similar activation patterns were recently reported by Chung *et al.*<sup>1</sup> Questions regarding the accessibility of these surface receptors to potential ligands prompted us to investigate ligand accessibility on a variety of frequently used basic biocompatible substrates for adherent cell imaging including bare glass (BG), fibronectin (FN), bovine serum albumin (BSA), fibronectinlike binding polymer (FNLP), collagen I, collagen IV, poly-*D*-lysine (PDL), and a commercially available basement membrane matrix called Geltrex™. For this particular work we opted not to use any acrylamide-based hydrogel preparations. While hydrogels are designed to have better ligand accessibility, standard preparations are too thick for most confocal and TIRF applications. Furthermore, there are only a few polymers that are easily modified for biocompatibility, and these produce substrates that scatter light and reduce the signal-to-noise (S/N) ratio to the detriment of quantitative image analysis applications. Microfluidics can be used to deliver ligands to specific locations of cells, but these substrates are not practical for image analysis techniques requiring uniform distribution of fluorescently labeled ligands on the cell surface.<sup>10</sup> Finally, while it is possible to use cell micropatterning or microcontact printing to create large channels with increased control over structure and chemical functionalization, the thin layers of gold that anchor the supportive islands preclude their use in TIRF imaging. Recently Kandere-Grzybowska *et al.*<sup>11</sup> developed an anisotropic solid microetching method, which could be used for TIRF, but we did not examine this type of support because it is not yet commonly used in TIRF and CLSM preparations.

As we hypothesized based on our confocal data of EGFR-eGFP activation in CHO-K1 cells, most of the biocompatible surfaces we examined restricted ligand accessibility to receptors on the basal membrane of well-adherent cells in standard 2D tissue cultures. Using binary analysis, we quantified the degree of propagation for a small dye molecule, Alexa 647 coupled to streptavidin, and the biotinylated epidermal growth factor (EGF) ligand coupled to the same dye. For both types of ligands and for all substrates we observed a higher degree of propagation under the peripheral regions of the cell (~5 μm from the cell edge) than the central regions of the cell. Coupling of a specific high affinity ligand to the dye resulted in a moderate increase in propagation for most substrates examined, at both the central and peripheral regions, even with the added bulk of the ligand. In control experiments, 20 nm carboxylate-modified FluoSpheres were completely excluded from the submembrane space. The observed steric and electrostatic limitations with respect to accessibility could be extended to larger probes and labels, including antibodies and quantum dots (QDs), making the

issue of reduced accessibility relevant to a large number of researchers who target protein or lipid components of the basal membrane.

## II. MATERIALS AND METHODS

### A. Cell culture

CHO-K1 cells expressing eGFP/EGFR constructs were generously provided by Jovin and Arndt-Jovin (Max Planck Institute for Biophysical Chemistry, Göttingen, Germany). Cells were cultured in Dulbecco's modified Eagle's medium, supplemented with 10% fetal bovine serum, 4 mM L-glutamine, 100 units/ml penicillin, 0.1 mg/ml streptomycin, 0.1 mM nonessential amino acids, and 0.5 mg/ml G418 to maintain transfection (Gibco, Carlsbad, CA). Cells were maintained in a humidified, 5.0% CO<sub>2</sub> atmosphere at 37 °C. For imaging cells were plated in Petri dishes with a bottom coverslip (CS) insert (No. 1.5; MatTek, Ashland, MA).

### B. Substrate preparations

Geltrex™ was purchased from Gibco/Invitrogen (Burlington, ON), while all other substrate materials were purchased from Sigma Aldrich Canada (Oakville, ON). Fibronectin, fibronectin engineered polymer, bovine serum albumin, and poly-*D*-lysine coated dishes were prepared by diluting to the appropriate concentration in phosphate buffered saline (PBS) without Ca<sup>2+</sup>/Mg<sup>2+</sup>. Following dilution, 1.5 ml of the solution was placed in a MatTek chamber and incubated at 37 °C for 1 h. After 60 min the samples were rinsed twice with PBS. Thin film preparations of Geltrex were made as directed by the supplier. Briefly, the Geltrex stock was thawed overnight at 4 °C. A solution of 100 μg/ml Geltrex was prepared in ice cold PBS, and 1.0 ml of the Geltrex solution was placed in the MatTek dish and swirled to evenly coat the dish. Dishes were placed in the incubator at 37 °C for 60 min. After 60 min the samples were rinsed twice with PBS. Collagen I and IV dishes were prepared by diluting acidified collagen stock solutions in PBS buffer to obtain the desired concentration, then 1 ml of solution was placed in the MatTek dishes. Dishes were placed uncovered in the incubator for 24 h to allow slow evaporation of the buffer. After 24 h the dishes were removed and rinsed twice with PBS.

Freshly passaged cells were diluted ~1/10 for 48 h adhesion assays. Into each coated dish 2 ml of Dulbecco's modified eagle medium growth media were added along with two drops of suspended diluted CHO-K1 EGFR-eGFP cells. Cells were incubated in a normal growth medium for 48 h. Prior to imaging the growth medium was removed, the cells were rinsed twice with PBS, and 1 ml of imaging medium (phenol red, fetal bovine serum, and geneticin free) was added. The cells were placed back in the incubator for a minimum of 2 h before microscopy imaging.

### C. Dye, ligand, and FluoSphere preparations

Nonspecific (NS) dye propagation assays were carried out with Alexa Fluor 647 streptavidin conjugate, Invitrogen Canada. A working stock solution of 20 μg/ml was pre-

pared from the 1000  $\mu\text{g}/\text{ml}$  stock solution using an imaging medium. This solution was then added to the cell dishes containing a 1 ml imaging medium to yield a final concentration of a 3.3  $\mu\text{g}/\text{ml}$  dye.

Specific dye propagation assays were carried out using a commercially available EGF-Alexa Fluor 647 streptavidin complex, Invitrogen Canada E35351. A working stock solution with a concentration of 6.8  $\mu\text{g}/\text{ml}$  was prepared by diluting the 200  $\mu\text{g}/\text{ml}$  original stock solution. To compensate for the differences in initial stock concentrations, we had to remove 800  $\mu\text{l}$  of the imaging medium from the cell dishes (leaving 200  $\mu\text{l}$ ) and then place 176  $\mu\text{l}$  of the diluted specific dye directly in the small imaging well. This allowed us to obtain the same final concentration (3.3  $\mu\text{g}/\text{ml}$ ) of ligand labeled dye as in the nonspecific assays.

Control measurements were carried out using 0.02  $\mu\text{m}$  diameter carboxylate-modified crimson (625/645) FluoSpheres<sup>®</sup>. Based on manufacturer provided specification, we prepared intermediate stock solutions of  $\sim 2.2 \times 10^{14}$  spheres/ml in an imaging medium. Next 200  $\mu\text{l}$  of this stock solution was added to cell dishes containing 1.0 ml of imaging medium to yield a final concentration of  $\sim 3.8 \times 10^{13}$  spheres/ml.

#### D. Analysis of accessibility

Determination of the percent propagation of NS dye or specific ligand labeled dye (S) was done using custom written image analysis programs in MATLAB (The MathWorks, Natick, MA). Whole cells, or regions of interest (ROIs) within a particular cell, were selected from the stack of images. Intensity threshold values for that region were input for channel I (green channel) and channel II (red channel). These threshold values were set as  $2\sigma$  above the photomultiplier tube (PMT) detector dark count noise for a given detection channel, where  $\sigma^2$  is the variance of the noise distribution. Each pixel was assigned a value of 1 or 0, corresponding to intensities above or below the respective intensity thresholds. The number of pixels containing values of 1 was multiplied by the pixel resolution to obtain the total area of the cell for the green channel. The same procedure was used in the red channel to determine the total area that contained dye molecules. We could then determine the percent propagation under the cell, or within a given region of interest. Confirmation of the accessibility was done by collecting a  $z$ -stack image series of the cell, and examining the space between the CS and the BM.

#### E. CLSM imaging

Cell samples were imaged using an Olympus FluoView FV300 (Olympus America, Melville, NY) confocal laser scanning microscope coupled to an Olympus IX71 inverted microscope equipped with a  $60\times 1.4$  numerical aperture oil immersion objective lens (Olympus PlanApo/IR). Cell samples with eGFP were excited with a 40 mW multiargon laser (458/488/515 nm, Melles Griot, Carlsbad, CA) using 10% power of a 40 mW 488 nm line. An Olympus FV-

FCBGR dichromatic beam splitter together with the emission interference and reverse interference filters BA510IF and BA530RIF (Chroma, Rockingham, VT) were used to efficiently reflect the 488 nm excitation wavelength and pass the emission wavelengths to the Channel I PMT. The Alexa 647 dye sample (Molecular Probes, Eugene, OR) was excited with 100% of a 10 mW, 633 nm helium-neon laser beam (Melles Griot, Carlsbad, CA). The beam splitter DM630 together with the emission interference filter BA660IF were chosen to efficiently collect and detect the Alexa 647 fluorescence emission via the channel II PMT. All images were  $1024 \times 1024$  pixels in size, with a pixel size of 0.0921  $\mu\text{m}$ . For each sample, an optimal setting of the laser power and PMT voltage was chosen to minimize pixel saturation and photobleaching. The CLSM settings were kept constant for all samples and controls (selection of filters, dichroic mirrors, scan speed, pinhole, and the step size for  $Z$ -stacks) so that valid comparison could be made between measurements from different data sets. Acquisition parameters were set within the linear range of the PMT photon detectors.

Focusing for experiments was achieved by first visually locating the basal membrane of the cells, and then taking an  $XYZ$  image series stack by moving away from the cell toward the coverslip in 0.2  $\mu\text{m}$  increments until scatter from the laser in channel II was maximized. We determined the number of steps between the maximum coverslip scatter signal and the basal membrane (four or five steps corresponding to 0.8–1.0  $\mu\text{m}$ ). We then positioned the focus half way between the measured distances using the automated axial positioning. The  $XYT$  image series were collected using the fast scan speed (2  $\mu\text{s}/\text{pixel}$ ) with a delay of 30 s between sequential images. The first scan was collected in the absence of the dye/ligand. Once this image was collected the appropriate amount of concentrated dye/ligand was added carefully to the imaging dish.  $XYZ$  image series stacks were collected using a 0.2  $\mu\text{m}$  step size, starting at least 1  $\mu\text{m}$  below the glass surface and continuing until the apical membrane became visible in the image.

### III. RESULTS AND DISCUSSIONS

Figure 1 presents CLSM fluorescence images of a typical nonuniform receptor clustering pattern following ligand treatment observed for CHO-K1 cells stably expressing an EGFR-eGFP construct. Cells were serum starved for 16 h prior to imaging to yield a homogeneous distribution of the fluorescently labeled EGFR on the cell surface [Fig. 1(a)]. Addition of a 100 nM EGF ligand consistently resulted in a large cell-to-cell variability [Fig. 1(b)] with respect to ligand-induced activation and clustering of EGFR on the basal membrane, as observed previously by ourselves and others.<sup>1</sup> Mainly we noted significant clustering of EGFR at the peripheral regions ( $\sim 5$   $\mu\text{m}$  from the edge) of highly adherent cells, and very little clustering occurring in the central regions. Additionally, limited overall clustering was observed for cells exhibiting moderate adhesion to the substrate (round shaped cells). We propose that the limited clustering in the central regions of the cells is due to reduced ligand accessi-

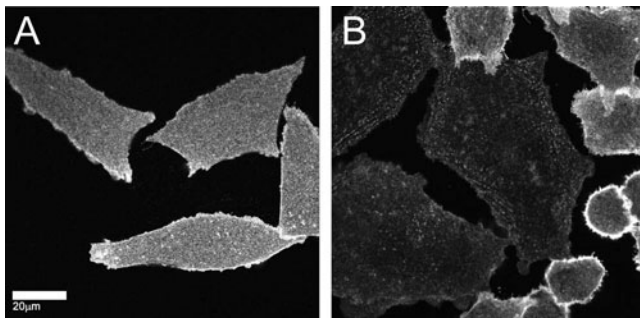


FIG. 1. Motivation obtained from EGFR activation patterns. Representative confocal images of adherent CHO-K1 cells stably expressing EGFR-eGFP prior (a) to and 6 min after stimulation with 100 nM EGF (b). Prior to stimulation with EGF ligand we have homogeneous distribution of EGFR-eGFP on the basal membrane. Following stimulation we consistently observe activation of the EGFR at the edges of well-adhered cells. Additionally, cells that appear to be weakly adhered (round shape) do not exhibit EGFR activation.

bility to the surface receptors on the basal membrane, due mainly to steric limitations, which reduce ligand access. The fluorescence images in Fig. 2 illustrate the limited accessibility for a nonspecific organic dye (Alexa 647 streptavidin) under the basal membrane of CHO-K1 cells expressing EGFR-eGFP. Visual comparison of the images in Figs. 2(a)

and 2(b) suggests good propagation of the dye at the edges of the large well-adhered cell, denoted as areas 2 and 4, and limited propagation under the smaller less-adherent cells (areas 5–7). Moreover, one can notice that the spatial profile of the fluorescence collected from the basal membrane in channel II reveals the positioning of cell adhesion sites. This indirectly confirms that the collected signal is specific to the Alexa 647 located underneath the cell (not signal bleedthrough from above the cell). Area 1 is an empty area outside of the cell, which was used as a reference point for maximum ligand propagation. Using both *XYT* and *XYZ* image scans we were able to quantify the degree of propagation for small NS dye under the basal membrane. Figure 2(f) is a mean intensity time trace recorded for each of the selected regions of interest, which reports on the ligand propagation. Here we note that only areas 2 and 4 show significant increases in intensity, and only a very small increase in overall intensity was noted for regions 5 and 7. The mean intensity time traces of the central region of the large cell (area 3), and under the rounded cell (area 6) show that the intensity does not increase above the PMT noise in these two regions. These findings were corroborated by examining of *XYZ* stacks for the same ROIs, taken 10 min postdye addition, and quantifying the mean intensities for each ROI in the stack.

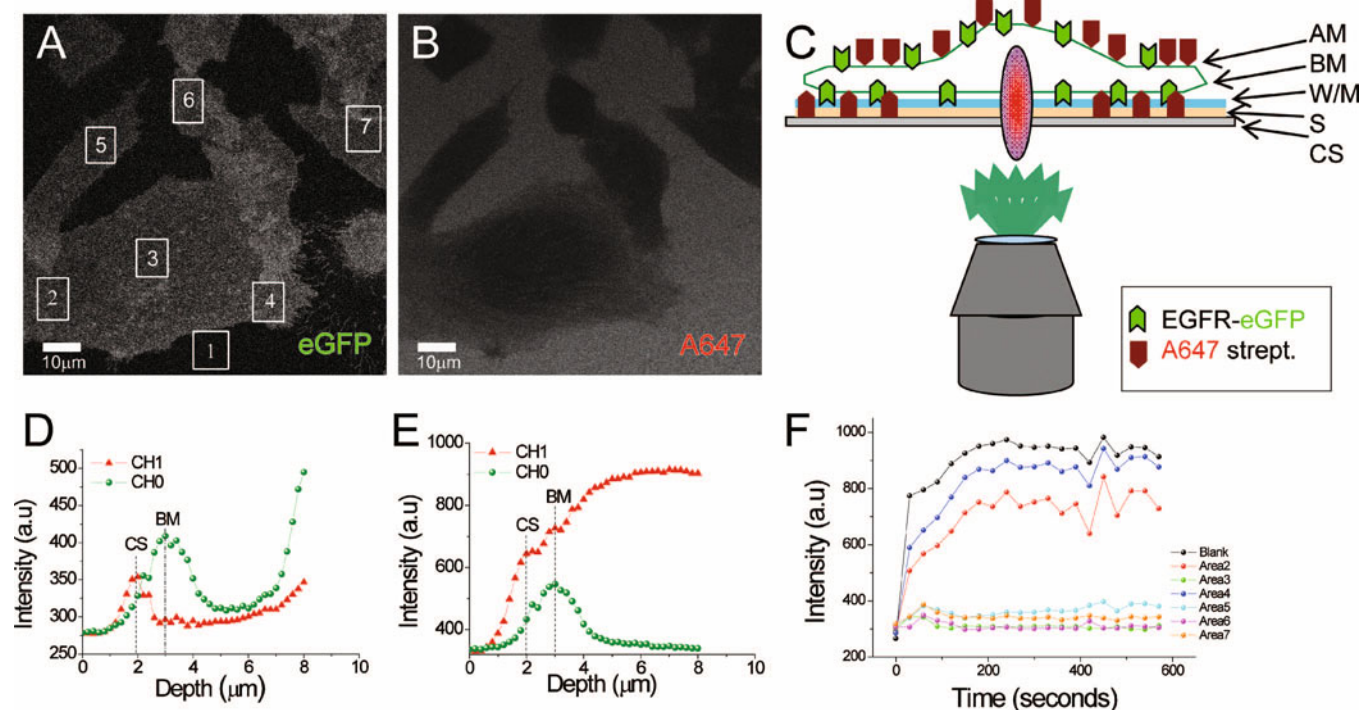


FIG. 2. (Color) Experimental conditions and initial observations. (a) EGFR-eGFP expressing cells plated on 0.5% BSA prior to addition of dye, recorded in channel 0. (b) Subsequent image recorded in channel 1 60 s after the addition of AlexaFluor 647 Streptavidin conjugate. (c) Cartoon depiction of the area of interest. CS—coverslip, S—substrate, W/M—water or media layer, BM—basal membrane, and AM—apical membrane. Note that we aim to image in the space between the substrate (S) and BM. [(d) and (e)] Integrated mean intensity traces obtained from *z*-stacks ( $0.2 \mu\text{m}$  step size) of areas 3 and 4, respectively. We record a sharp spike in intensity in channel 1 attributed to reflections arising from changes in refractive index values at the coverglass interface. This spike is denoted as CS on the mean intensity traces. Moving further into the sample we reach the maximum signal arising from the EGFR-eGFP on the basal membrane of the cells recorded in channel 0, and denoted as BM on the mean intensity traces. To obtain images demonstrating the propagation such as the one shown in panel (b) we would position the sample at an equal distance between the identified CS and BM areas,  $\sim 0.5 \mu\text{m}$  above the coverglass. Comparison of the integrated mean intensity traces for regions 3 and 4 indicated a greater degree of propagation of the AlexaFluor 647 conjugate for area 4, as expected from visual inspection of panel (b). (f) Real time traces of integrated intensities recorded in channel 1 for each of the selected ROIs.

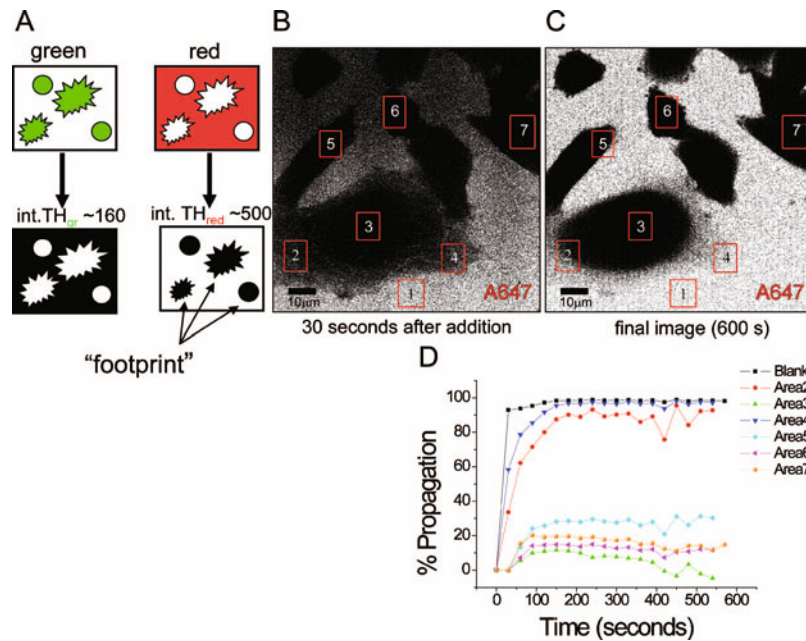


FIG. 3. (Color) Binary image analysis method. (a) Cartoon representing the binary analysis methodology. Representative confocal images of Alexa 647 dye localized under the basal membrane of CHO-K1 cells 30 s (b) and 10 min (c) after addition of the dye. (d) The resulting percent propagation curves obtained from each of the ROIs shown in Fig. 2. As noted in Fig. 2(f), minimum propagation of the dye is observed in the central regions of the large cell and the peripheral regions of less-adherent cells.

Mean intensity versus image  $z$  position traces for regions 3 and 4 are given in Figs. 2(d) and 2(e), respectively. For area 3, the central region of the cell, we note that there is no dye accumulated between the CS and the BM, while the peripheral region (area 4) shows a significant amount of dye accumulation.

For this investigation we chose to use CLSM rather than TIRF for three reasons: (1) CLSM provides a more uniform spatial illumination profile across the field of view, (2) each of the prepared substrates used would have slightly different thicknesses, and confocal imaging allows us to focus in the small subcellular location independent of substrate thickness and morphology, and (3) confocal optical sectioning allows us to obtain  $z$ -stacks of the cells to verify the results obtained with time series on the basal membrane.

Initially we analyzed the data sets collected in channel II with spatial ICS,<sup>8</sup> in an attempt to quantify the number density of the dye propagated under a cell over the course of imaging. We abandoned this type of analysis for a number of reasons. Spatial ICS would provide us with the measure of the accumulation of dye (number of dyes per beam area) and would not quantify the degree of propagation (fraction of the cell area, which is also occupied by the dye). Moreover, the dye accessibility varies significantly depending on the area of the basal membrane (peripheral versus central). The resulting gradient in spatial fluorescence intensity of a given ROI made it impossible to recover unbiased number densities from spatial ICS due to the deviation from homogeneity. To avoid these artifacts, we adopted a binary analysis method to efficiently estimate the degree of propagation in the presence of photobleaching for long collection times. A cartoon representation of the binary analysis is given in Fig. 3(a).

Briefly, regions of interest within a particular cell were selected from the stack of images. Intensity threshold values for that region were input for the green and red channels. These values were set as  $2\sigma$  above the mean value of the background intensity in the image for the corresponding channel. We observed a higher level of background noise in channel II as compared to channel I, due to stronger reflection of the laser at the coverslip/substrate interface. By comparing the two stacks of images we were able to quantify the percent propagation within the ROI. Figures 3(b) and 4(c) are sample CLSM images obtained in channel II (red channel) at 30 s and 600 s after addition of NS dye (Alexa 647 streptavidin). The percent occupancy for each of the ROIs indicated is shown in Fig. 3(d). It is important to note that we normalize the percent occupancy curves for each region by assigning the control area outside of a cell (given here as area 1) a value of 100% propagation. This was done to obtain results that would be unbiased by the electrostatics of the different surfaces examined. At physiological  $pH$ , FN and BSA carry a negative charge, collagen substrates carry a small positive charge, and the remaining substrates carry a large positive charge. While cells prefer to interact with positively charged surfaces, the organic dye distribution varied with respect to surface charge, and thus a correction was needed to compare results on different substrates. While the graphs shown in Figs. 2(f) and 3(d) appear to be similar, the binary analysis method [Fig. 3(d)] is more sensitive to the presence of low effective concentrations of dye (ligand) than simply plotting the average integrated intensity for a given region. With the use of binary analysis, we measure a small

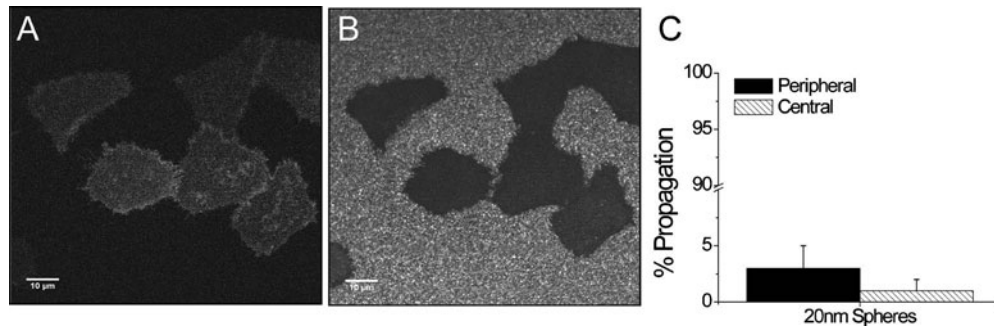


FIG. 4. Fluorescent microsphere control measurements. Confocal images acquired in green (a) and red (b) channels of EGFR-eGFP expressing cells plated on a bare glass with 20 nm (diameter) FluoSpheres added to the imaging media. (c) The average percent propagation was found to be  $2 \pm 2\%$  and for the central regions of the cells the propagation was found to be  $1 \pm 1\%$ . The average intensity measurement in the blank area was  $1100 \pm 200$  counts. For comparison, a typical assay using AlexaFluor 647 yielded an average intensity of  $600 \pm 200$  counts in a typical blank region. Similar results were obtained for all substrates (data not shown).

increase in the percent propagation for all areas of interest, even within area 3 the central region of the larger adhered cell.

Binary analysis had an additional benefit of being less susceptible to artifacts introduced by photobleaching. Under our experimental imaging conditions, the rate of photobleaching was not sufficient to reduce the signal in either channel below the set intensity threshold values. Moreover, areas such as the edges of cells where substantial amounts of dye/ligand accumulate would significantly bias the obtained values of occupancy using integrated intensity or spatial ICS measurements.

Control measurements were carried out using a saturating concentration of 20 nm diameter FluoSpheres, which we did not expect to propagate under the basal membrane due to steric constraints. Sample CLSM images of EGFR-eGFP cells plated on a bare glass with beads added to the imaging buffer are shown in Fig. 4. Here we observe that the 20 nm FluoSpheres are excluded from the subbasal membrane space. Using binary analysis we detect only  $2 \pm 2\%$  combined propagation and only  $1 \pm 1\%$  propagation in the central regions of the cells. Based on these measurements we are confident that the measured signal we obtain for the dye propagation assays does not arise from fluorescence in the bulk solution above the apical membrane of the cell.

Using binary analysis we systematically examined the degree of NS Alexa 647 dye propagation under the basal membrane for CHO-K1 cells expressing EGFR-eGFP plated on a variety of commonly used substrates. We characterized the accessibility of both the central and peripheral regions. Sample confocal images for the NS propagation in the green and red channels are given in Figs. 5(a) and 5(b). Similar images were obtained for all the surface types examined [Figs. 5(d) and 5(e), surfaces  $x$  and  $y$ , respectively]. A summary plot of the percent propagation obtained using binary analysis for each of the surfaces is given in Fig. 5(g), and a summary of the average values is presented in Table I. The reported concentrations for each of the substrates were determined to be optimal for nonspecific propagation based on experiments carried out using a series of different concentra-

tions. The resulting graphs for each of the substrates prepared at different concentrations are shown in Fig. 6.

Inspection of Fig. 5(g) shows clearly that for the central regions of the cells there is very little propagation of the dye under the basal membrane. For cells plated on a bare glass the average propagation under the central region was found to be only  $8 \pm 0.5\%$ , demonstrating a strikingly low accessibility. The highest propagation values for central regions were obtained using FNLP and Geltrex™ with values of  $42 \pm 4.2\%$  and  $45 \pm 4\%$ , respectively. Fibronectinlike protein polymer (Sigma) is a synthetic positively charged polymer that has multiple copies of the arginyl-glycyl-aspartyl binding epitope embedded in the peptide units. These peptides adopt a very stable IIID conformation. Geltrex™ (Invitrogen) is a purified soluble basement membrane matrix consisting mainly of laminin, collagen IV, entactin, and heparin sulfate proteoglycan. Geltrex™ is a basement membrane mimetic generating a three-dimensional (3D) structural support surface on which cells can be cultured. Geltrex™ was chosen because it is essentially a natural hydrogel that can be used with a thin preparation method suitable for TIRF and confocal studies. While both of these substrates provided substantially better accessibility to the central regions of cells, there was still a significant portion of the subcellular/extracellular matrix (ECM) space in which the dye did not freely propagate.

We were interested to know if there would be enhanced propagation of the dye if it was coupled to a ligand specific for a surface receptor expressed at the plasma membrane. To determine if there was a specific ligand effect we used biotin-streptavidin coupling to examine the degree of propagation for EGF coupled to Alexa 647. The results are shown in Fig. 5(f), and a summary of the measured percent propagation values is presented in Table II. Upon comparison of Figs. 5(c) and 5(f) it is immediately apparent that when the Alexa 647 streptavidin is coupled via biotin to EGF there is an increase in propagation in both the central and peripheral regions of the cells on all substrates examined, except on Geltrex and FNLP, which remained the same within error, as shown in Fig. 5(g). For both FN- and BSA-coated coverslips

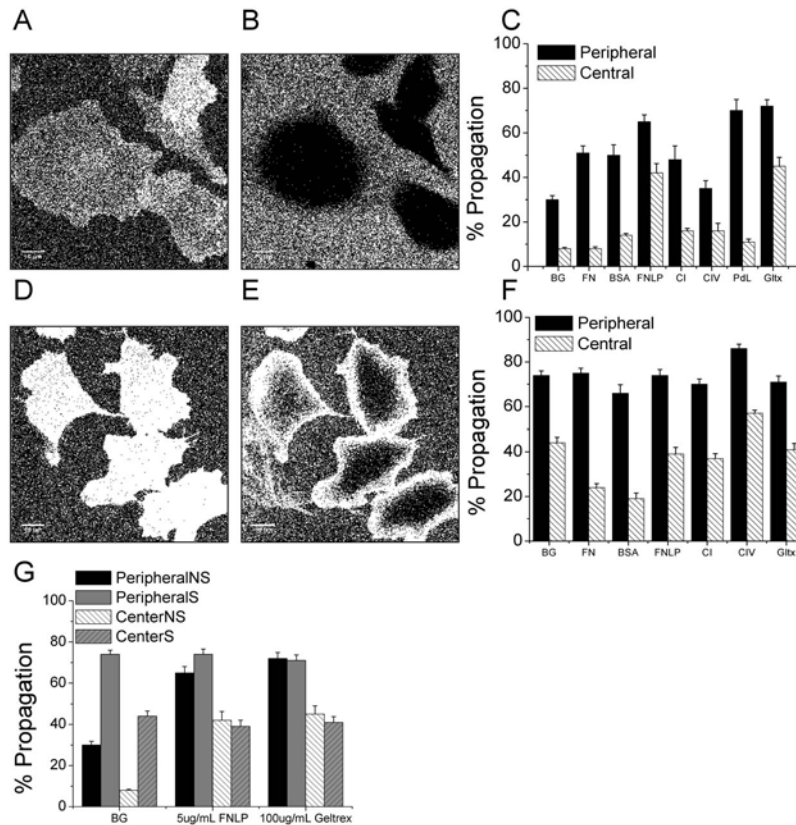


FIG. 5. Specific versus nonspecific propagation measurements. Green (a) and red (b) channel binary images for nonspecific propagation of AlexaFluor 647 dye for EGFR-eGFP stably expressing CHO-K1 cells plated on 5  $\mu\text{g}/\text{ml}$  FN at 9.5 min postaddition of the dye. Green (d) and red (e) channel binary images for specific ligand propagation of AlexaFluor 647 Streptavidin—biotin EGF for the cells plated on 5  $\mu\text{g}/\text{ml}$  FN. The results of the binary image analysis applied to the nonspecific (c) and EGF ligand specific (f) data obtained for various substrates. (g) The summary plot of the percent propagation obtained using binary analysis for each of the surfaces.

the increased propagation in the central regions was not as significant as for bare glass and collagen substrates. To further highlight the increase in specific ligand propagation for cells plated on a bare glass we directly compared the S and NS propagations of Alexa 647 at the central and peripheral regions with the values obtained for both Geltrex<sup>®</sup> and FNLP, shown in Fig. 5(g). While we observed a significant improvement in the overall accessibility under CHO-K1 cells plated on a bare glass for the specific binding, the measured propagation within the central region of the cells was still less than 50%. These findings suggest that high affinity interaction between EGF and EGFR ( $K_D \sim 1$  nM) is still not enough to overcome potential steric and electrostatic barriers present in the subbasal membrane space of adherent cells plated on a bare glass.<sup>12,13</sup>

CHO-K1 cells are commonly used in cell migration studies as they are adherent and form strong adhesions. Robust adhesions, which are formed by cells after 48 h, result from the cells excreting their own ECM; in the case of CHO-K1 cells this is predominantly FN.<sup>14,15</sup> Consequently, in addition to the initial substrate used to coat the coverglass, the CHO-K1 cells are able to modify the surface by excreting ECM proteins and carbohydrates. Interestingly, despite the fact that cells alter their environment in this way we still see differences in accessibility to the basal membrane on the

different coatings, which suggests that even after 48 h they maintain characteristics of the initial surface coating. Based on the fundamental physical-chemical characteristics of the substrates, we had postulated that we would see the greatest subcellular propagation of dye/ligand for those which had a more pronounced 3D structure, such as fibril collagen,<sup>16</sup> sheet collagen (IV), FNLP, and Geltrex<sup>™</sup>, as compared to FN and PDL, which are not known to self-assemble in an organized manner. Human fibronectin exists at physiological pH in a compact globular structure<sup>17</sup> while BSA has been shown to adsorb in a multilayer fashion at pH values above

TABLE I. Summary of propagation data for nonspecific dye studies.

Substrate	<i>N</i>	Overall	Peripheral	Central
Glass	120	25 ± 1.9	30 ± 1.7	8 ± 0.5
FN 5 $\mu\text{g}/\text{ml}$	60	36 ± 3.7	51 ± 3.1	8 ± 0.8
BSA 0.25%	30	44 ± 5.0	50 ± 4.6	14 ± 0.8
FNLP 5 $\mu\text{g}/\text{ml}$	50	60 ± 3.6	65 ± 3.1	42 ± 4.2
Collagen I 10 $\mu\text{g}/\text{ml}$	30	37 ± 6.3	48 ± 6.1	16 ± 1.1
Collagen IV 10 $\mu\text{g}/\text{ml}$	30	29 ± 4.1	35 ± 3.5	16 ± 3.4
PDL 100 $\mu\text{g}/\text{ml}$	30	55 ± 3.4	70 ± 5.0	11 ± 1.3
Geltrex <sup>®</sup> 100 $\mu\text{g}/\text{ml}$	70	67 ± 8.2	72 ± 2.9	45 ± 4.0

The values presented here are the average of all the areas sampled ± SEM.

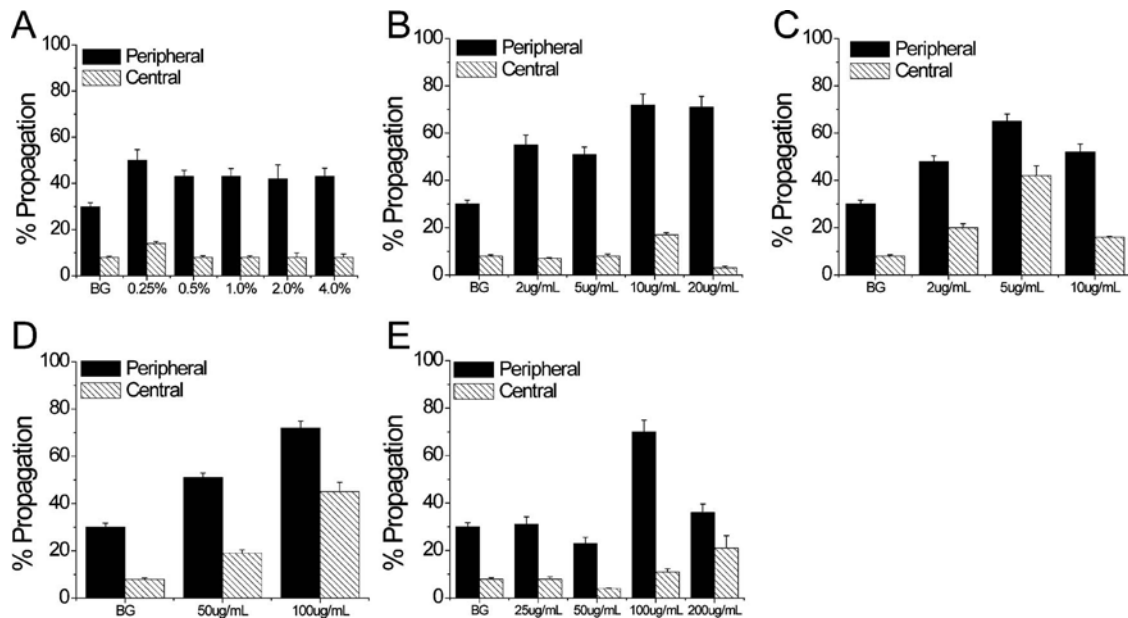


FIG. 6. Ligand propagation data for different surface preparation conditions. (a) BSA. (b) FN. (c) FNLP. (d) Geltrex. (e) PDL.

its isoelectric point (4.7), which could provide sufficient spacing to allow diffusion of larger molecules.<sup>18</sup> Intuitively, one would expect that any substrate that provides a 3D porous support for the cells would result in less constrained subcellular diffusion of dye and ligand molecules. The most promising substrate based on our investigation was the commercially available Geltrex™ basement membrane matrix. The porous mesh of basement membrane components coupled with the ECM excreted by the CHO-K1 cells resulted in the most optimal free diffusion under our experimental conditions. For this investigation we used a thin layer preparation in order to meet ideal thickness criteria for CLSM and TIRF applications. Thicker preparations may result in increased propagation of species through the gel, but we did not investigate these due to decreased S/N and increased scattering when imaging. While full characterization of each of the substrates described here is beyond the scope of this current study, an increased understanding of the organization and distribution of each of the substrates adsorbed on glass surfaces would aid in further elucidating the contributions of the steric and electrostatic forces, which govern ligand propagation at the basal membrane of adherent cells.

We have found no prior studies examining the correlation between the diffusion of particles between the basal membrane of adherent cells and biocompatible substrates on which the cells are plated. Accurately describing diffusive behavior in such a confined environment is a complex problem that cannot be modeled using simple Smoluchowski–Einstein theory.<sup>19</sup> There is, however, a large number of studies examining free diffusion of particles through 3D biopolymers, with implications for tissue engineering. Perhaps the best studied biopolymer is the ECM, which *in vivo* facilitates the transport of nutrients, oxygen, and small mol-

ecules (including growth factors) via diffusion, but also acts as a physical barrier due to the organization and density of the components within the ECM itself. In addition to physical size limitations on diffusion through the ECM, Lieleg *et al.*<sup>13</sup> demonstrated that there is a strong degree of electrostatic filtering, which can further inhibit the diffusion of charged species, regardless of size.

Ellis<sup>12</sup> examined the effects of molecular crowding and macromolecular confinement within cells, but it is reasonable to expect similar behavior in the crowded and narrow space between the substrate and a well-adhered cell. Ellis determined that crowding affects both reaction rates and equilibrium, and these results exhibited nonlinear behavior with respect to the probe size chosen. The main consequence of macromolecular crowding is that there is a difference between the effective and actual concentration of ligands, and thus concentration is more accurately reflected using an ac-

TABLE II. Summary of propagation data for specific dye studies.

Substrate	<i>N</i>	Overall	Peripheral	Central
glass	100	68 ± 2.4	74 ± 2.0	44 ± 2.5
FN 5 μg/ml	100	66 ± 2.9	75 ± 2.2	24 ± 1.8
BSA 0.25%	40	57 ± 4.8	66 ± 3.8	19 ± 2.5
FNLP 5 μg/ml	80	67 ± 3.1	74 ± 2.6	39 ± 3.0
Collagen I 10 μg/ml	40	63 ± 3.2	70 ± 2.3	37 ± 2.2
Collagen IV 10 μg/ml	30	81 ± 3.3	86 ± 2.0	57 ± 1.4
PDL 100 μg/ml				
Geltrex® 100 μg/ml	60	65 ± 3.1	71 ± 2.7	41 ± 2.8

The values presented here are the average of all the areas sampled ± SEM.

tivity coefficient (or thermodynamic activities). Based on our findings we would expect the same to be the case for ligands/probes under the basal membrane of cells. Rather than assuming that all the ligands can propagate, one should use the effective concentration rather than the actual concentration. Moreover, the crowded environment between the basal membrane and coverslip can result in a large excluded volume. Under this regime, the activity of the ligand would be much higher than in the bulk solution, and interactions between ligands in this crowded space can further complicate equilibrium reactions. Consequently it is expected that for diffusion-limited reactions (e.g., EGF binding to EGFR) macromolecular crowding would result in an overall reduced rate of reaction by reducing diffusion and access to reactive sites of surface receptors. However, if some of the ligand molecules do encounter the reactive site, an increase in the reaction rate is expected due to decreased conformational entropy for each ligand. This would explain why we note fast and efficient clustering of EGFR at the edges, and not at the central regions of cells (Fig. 1). For reactions that are activation limited one would expect that the effects of macromolecular crowding would not be as significant, and thus would be less affected by reduced ligand propagation.<sup>12,20</sup> Based on our findings and diffusion studies in literature, one should expect that both propagation and molecular crowding should be considered when attempting to quantitatively study ligand-receptor binding on the basal membrane of adherent cells. This is particularly true for temporal studies on diffusion-limited reactions. Under these conditions one would expect that there would be significant peripheral activation/binding but limited stimulation in the central regions of cells. Further, any observed changes in receptor distribution in the central region may be a result of downstream activation rather than direct stimulation, and thus care should be taken when calculating binding constants and rate constants for reactions based on data collected in these regions.

Similar peripheral EGFR-eGFP activation patterns as observed in Fig. 1 were noted by Chung *et al.*<sup>1</sup> They concluded that the enhanced EGFR-eGFP dimerization at the peripheral regions of adherent mammalian (CHO-K1) cells was due to larger amounts of preformed dimers available for binding in this specific region of the cell. While their results suggest that preformed dimers exhibit enhanced EGFR-EGF binding, the limited activation of EGFR-eGFP in the central regions of the cells may be due to limited propagation of the QD-labeled ligands under the basal membrane of these highly adherent cells.<sup>1</sup> Core-shell QDs with biocompatible coatings typically have diameters on the order of  $\sim 25$  nm, which is significantly larger than small organic molecules, which have diameters on the order of  $\sim 1.7$  nm, so it is not unlikely that QD probes would exhibit anomalous diffusion and limited propagation beyond the peripheral region of cells.<sup>19</sup> In fact, it has been shown that QD probes have significantly slower diffusion than organic fluorophores in small areas such as synapses.<sup>21</sup> Moreover, quantum dots should always be treated as colloids due to their large surface charge, and based on the work by Lieleg *et al.*<sup>13</sup> one would expect the

ECM secreted by adhered cells to further preclude full access of the QD probes to the central regions of cells.

#### IV. CONCLUSIONS

When examining the basal membrane of adherent cells one cannot take for granted that all areas of the cell will be accessible, and further the reduced accessibility of probes/ligands to all areas of the cells may alter the rate of diffusion-limited reactions. All biocompatible substrates we examined exhibited limited accessibility of ligands to the central regions of the basal membrane of adherent cells. Our findings impact many types of quantitative imaging and analysis techniques, which often examine sections of the basal membrane of cells plated on various substrates but implicitly assume homogeneous ligand properties across the entire cell. The most promising commercially available substrates we examined were Geltrex<sup>TM</sup> and fibronectin engineered polymer; however, even on these substrates some cells remained inaccessible to ligands/dye. The presence of a specific ligand for EGFR resulted in increased propagation under the cell despite the added bulk, suggesting that simple passive diffusion is not the limiting factor in ligand propagation. Our study highlights the need to develop improved ultrathin porous biocompatible substrates with well-characterized structural properties on the nano- and micrometer length scales for use with basal membrane studies on adherent cell lines (CHO, HeLa, etc.).

#### ACKNOWLEDGMENTS

The authors acknowledge T. M. Jovin and D. Arndt-Jovin (Max Planck Institute for Biophysical Chemistry) for providing the transfected CHO cell line used in these studies. They thank funding in support of this work from the Natural Sciences and Engineering Research Council of Canada (NSERC), the Canada Foundation for Innovation (CFI), and the Canadian Institutes of Health Research (CIHR). J.L.S. acknowledges financial support from a NSERC postdoctoral fellowship.

<sup>1</sup>I. Chung, R. Akita, R. Vandlen, D. Toomre, J. Schlessinger, and I. Mellman, *Nature (London)* **464**, 783 (2010).

<sup>2</sup>C. Brown, B. Hebert, D. Kolin, J. Zareno, L. Whitmore, A. Horwitz, and P. Wiseman, *J. Cell. Sci.* **119**, 5204 (2006).

<sup>3</sup>M. Sergeev, S. Costantino, and P. Wiseman, *Biophys. J.* **91**, 3884 (2006).

<sup>4</sup>T. Gadella, Jr. and T. Jovin, *J. Cell Biol.* **129**, 1543 (1995).

<sup>5</sup>S. Mukherjee, R. Ghosh, and F. Maxfield, *Physiol. Rev.* **77**, 759 (1997).

<sup>6</sup>P. Yeagle, *The Structure of Biological Membranes* (CRC, Boca Raton, FL, 2005), pp. 157–174.

<sup>7</sup>J. B. Pawley, *Handbook of Biological Confocal Microscopy*, 2nd ed. (Plenum, New York, 1995), pp. 327–355.

<sup>8</sup>N. Petersen, P. Höddelius, P. Wiseman, O. Seger, and K. Magnusson, *Biophys. J.* **65**, 1135 (1993).

<sup>9</sup>P. Wiseman, J. Squier, M. Ellisman, and K. Wilson, *J. Microsc.* **200**, 14 (2000).

<sup>10</sup>D. Huh, W. Gu, Y. Kamotani, J. Grothberg, and S. Takayama, *Physiol. Meas.* **26**, R73 (2005).

<sup>11</sup>K. Kandere-Grzybowska, C. Campbell, Y. Komarova, B. Grzybowski, and G. Borisy, *Nat. Methods* **2**, 739 (2005).

<sup>12</sup>R. Ellis, *Trends Biochem. Sci.* **26**, 597 (2001).

<sup>13</sup>O. Lieleg, R. Baumgärtel, and A. Bausch, *Biophys. J.* **97**, 1569 (2009).

<sup>14</sup>S. Johansson, G. Svineng, K. Wennerberg, A. Armulik, and L. Lohikangas

- gas, *Front. Biosci.* **2**, d126 (1997).
- <sup>15</sup>C. Chung and H. Erickson, *J. Cell. Sci.* **110**, 1413 (1997).
- <sup>16</sup>D. F. Holmes, H. K. Graham, J. A. Trotter, and K. E. Kadler, *Micron* **32**, 273 (2001).
- <sup>17</sup>D. E. MacDonald, B. Markovic, M. Allen, P. Somasundaran, and A. L. Boskey, *J. Biomed. Mater. Res.* **41**, 120 (1998).
- <sup>18</sup>O. Mori and T. Imae, *Colloids Surf., B* **9**, 31 (1997).
- <sup>19</sup>J. Szymański, A. Patkowski, A. Wilk, P. Garstecki, and R. Holyst, *J. Phys. Chem. B* **110**, 25593 (2006).
- <sup>20</sup>B. Yari, F. Khorasheh, and A. Kheirloomoom, *Chem. Phys.* **321**, 34 (2006).
- <sup>21</sup>L. Groc, M. Heine, L. Cognet, K. Brickley, F. A. Stephenson, B. Lounis, and D. Choquet, *Nat. Neurosci.* **7**, 695 (2004).